


A novel computer-aided tree-ring analysis software (CATS): oak earlywood vessel size reveals a clear spring heat sum response

Alexander Land¹  · Matthias Wehr² · Kai-Uwe Roelfs² · Simon Epkes² · Daniel Reichle¹ · Gerhard Kauer²

Received: 17 February 2017 / Accepted: 3 July 2017 / Published online: 8 July 2017
© The Author(s) 2017. This article is an open access publication

Abstract

Key message The use of cell-size parameters from oak trees as a powerful proxy for past climate reconstruction needs to be more intensively studied. The freeware tool CATS will help pushing these high-volume cell-size measurements.

Abstract In this study, we analyzed the response of vessel size chronologies to daily meteorological records. For this purpose, we developed a computer-aided tree-ring analysis software (CATS) for high-volume cell-size measurements. To stress test CATS, quantitative vessel parameters were measured in 22 living ring-porous oak trees from two riparian-like forests (Mainfranken, southern Germany). Climate response analysis was performed using daily meteorological records. To make the measurement of millions of such vessels within wooden samples feasible, semi-automated computer-aided software for high-volume analysis is crucial. To expedite the measurement of the cells within distinct tree rings, CATS was developed to enable the automated measurement of a high number of samples and tree rings. CATS uses common image segmentation techniques as well as novel software algorithms to detect earlywood vessel superclusters that are used to identify distinct tree rings. The software structure of CATS is described in detail. The climate–vessel response analysis

shows a clear temperature signal from mid-March to mid-April (March 14–April 18). This effect is particularly pronounced for a 50-year span in the twentieth century (1915–1964).

Keywords Quantitative wood anatomy · Temperature · Image analysis software · Microscopy

Introduction

Dendroclimatologists use classical tree ring proxies (ring width or maximum latewood density) to reconstruct climate variability from thousands of years ago with annual to seasonal resolution (Büntgen et al. 2011; Esper et al. 2013; Land et al. 2015; Schönbein et al. 2015; Seftigen et al. 2013; Wilson et al. 2013). These proxies are very common and an extensive network of tree ring series is currently available for the entire Northern Hemisphere (St. George 2014). For Central Europe, millennia-length tree-ring chronologies as well as many precisely dated wooden samples are available (Friedrich et al. 2004; Leuschner et al. 2002; Spurk et al. 1998) spanning the entire Holocene. These climate tree-ring archives are perfectly suited for investigations into past climate variability and environmental changes (Land et al. 2015; Land 2014; Schönbein et al. 2015; Spurk et al. 2002) on a spatio-temporal scale. Trees develop an immense number of earlywood vessels of varying size and shape every growing season, thus recording particular weather conditions. In the past decade, an increasing number of investigations have been performed to study the response of xylem cell anatomy and hydraulic architecture to environmental and climatic conditions (Fonti et al. 2010 and references therein; Land 2014) to generate climate

Communicated by A. Braeuning.

✉ Alexander Land
alexander.land@uni-hohenheim.de

¹ Institute of Botany (210a), University of Hohenheim, Garbenstraße 30, 70599 Stuttgart, Germany

² Bioinformatics, University of Applied Sciences, Constantiaplatz 4, 26723 Emden, Germany

proxies with a much higher resolution (down to monthly) compared to the classical proxies of ring width and maximum latewood density. Today, wood-anatomical variables (e.g., cross-sectional lumen area) are discussed as potential proxies for climate reconstructions (Fonti et al. 2010; Fonti and García-González 2008; Kniessel et al. 2015; Land 2014) to ensure monthly to seasonally resolved insights into past environmental changes. In contrast to the classical total-ring width proxy, the measurement of cell sizes within tree rings is strongly hindered by the time-consuming preparation process necessary to obtain a smooth cross-sectional surface of the wooden probes. Using wood-anatomical variables (e.g., mean annual cross-sectional vessel area) for climate reconstruction, a high number of correctly dated tree rings from ancient to living samples are needed to ensure a noise-free climate signal and to diminish the influence of tree-individual xylem hydraulic architecture of individual trees. High-volume analysis is therefore essential, necessitating measurements of millions of cross-sectional cells in a short time.

Here we present a computer-aided tree-ring analysis software (CATS) for the accurate, efficient and nearly fully automated measurement of earlywood vessel sizes in ring-porous tree species for mass data analysis. Reliable image segmentation is critical, which is a fundamental part of the methodology described here (Peng 2008) to distinguish vessels to be measured from uninteresting background structures, or also to recognize disturbances within objects of interest which should be eliminated. Deletion of falsely detected objects and the use of knowledge-based verification of identified shapes was implemented to expedite the detection of earlywood vessels within annual growth rings and to improve the measurement process. The algorithms used to achieve these goals as well as results of climate response analysis of vessel proxies using daily meteorological records are presented.

Materials and methods

Implementation

For our software development, we implemented the basic methods of OpenCv image analysis library (EmguCV wrapped, as we implemented our application in C#, Windows 64 bit). As our goal was to clearly detect earlywood vessels, we had to first complete a careful image segmentation based on several parameters, like vessel area, roundness factor and position of the vessels within tree rings. These parameters serve as a ‘model’ for our analysis. The program flowchart of CATS is shown in Fig. 1.

Image segmentation

24-bit color information was transformed down to 8-bit grayscale through simple $(R + G + B)/3$ reduction of the color channels. Following auto-contrast processing, we automatically adjusted the histogram in regard to image brightness and contrast to optimize conditions for subsequent image processing as it is difficult to achieve binary images which display the earlywood vessels in their original geometry with minimal interference. As this is one of the most critical steps for the end result, we added an iterative fine-tuning of the global brightness applied to the image in response to object detection and compared to our model of vessels at each iteration: in case the iterative step results in objects which fit better to our model for vessels, the previously determined brightness was then regarded as being sub-optimal. A fine-scaling was then performed within a certain window around the newly detected brightness value. The image was iteratively subjected to a threshold with the given values and the contours that resulted from the step measured for five positions within the newly defined brightness window. For each step, object detection was applied to measure the vessels geometry and size. These values were again compared to our model of vessels. The best result of each iteration process was chosen (geometry of “potential vessels” is one criterion in addition to the area), but was once again regarded as sub-optimal for the next iteration with a much tighter window spanned around that value. It was demonstrated that no more than three such iterations were necessary to achieve the best and final value for brightness, which did not overly affect earlywood vessel geometry when Otsu’s (1979) thresholding was applied. In the next step, the diversity of gray scale information was reduced to produce the final binary image in order to detect vessels within. To automatically compute a threshold, we used histogram accumulation. We used an empirically determined window of 30% for the bright and 0.5% for the dark section of the accumulated histogram for binning in two pixel classes.

The result of this accumulated histogram, the maximum of the intra-class variance, was chosen for conducting Otsu’s thresholding operation on the image. This generated a two-level image that was used to finally detect the contours of all white objects. The major problem with binary images generated through this operation after Otsu is that many disturbances and structures remain which are not actually vessel lumen (Fig. 2).

Another challenge arises regarding structures within the vessels which could lead to incorrectly measured cross-sectional areas (Fig. 2).

To remove smaller disturbances and achieve an overall smoothing of vessel borders, we used a combination of opening- and watershed-based dilation (Cousty et al. 2006)

Fig. 1 Program flowchart of CATS. General steps processed for segmentation, detection and finally clustering the vessel objects within the given image. The object model behind is defined by the geometry of an ‘ideal’ vessel (known by experience) and the histological structure of a tree ring (by distances and orientation of vessels)

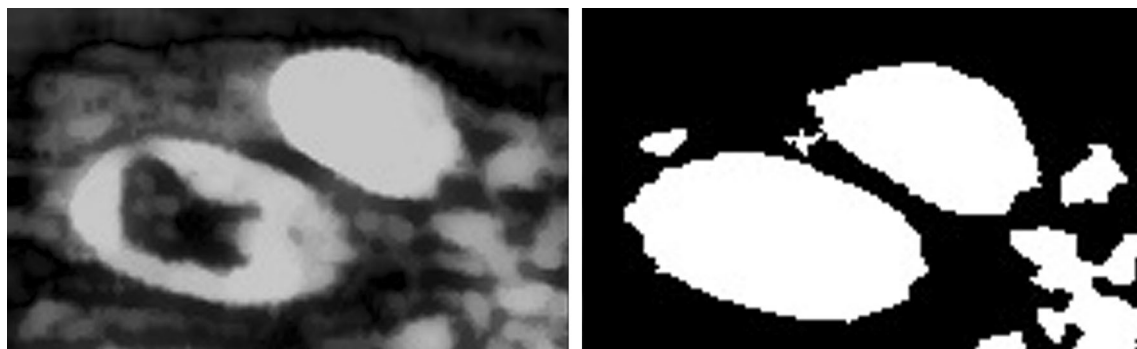
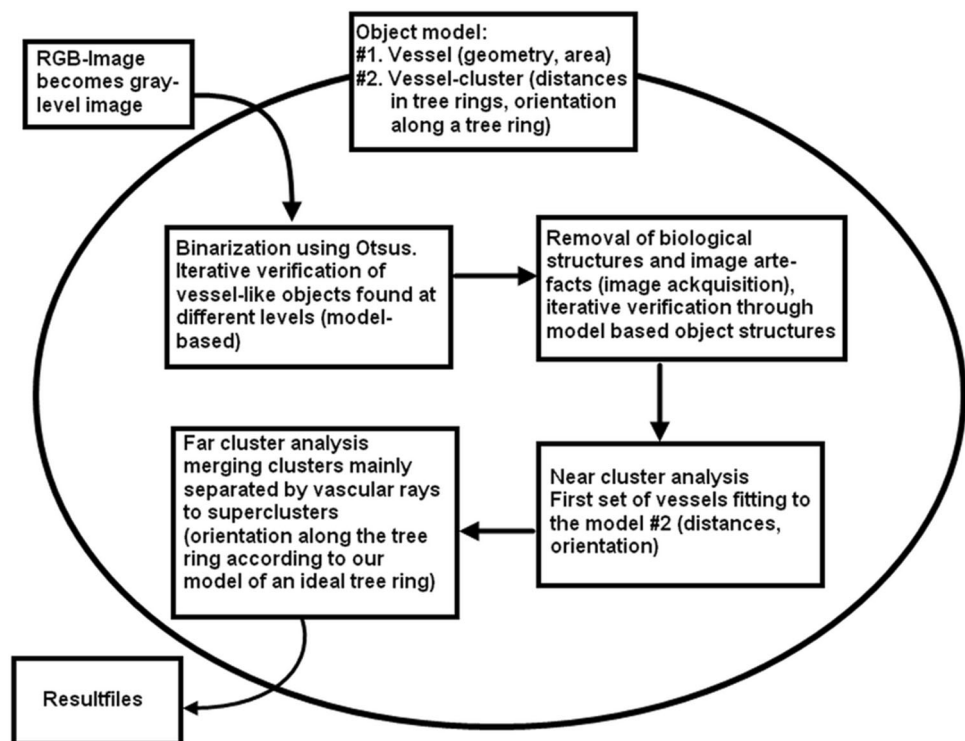


Fig. 2 The original image shows an intra-cellular artifact within the lower left earlywood cell. After standard thresholding (operator after Otsu (1979), accumulated histogram interpretation), a binary image is

generated and the tylosis structure eliminated using the watershed procedure during an applied dilation routine. If these artifacts are not removed, they will cause errors in area measurement

prior to the application of the last step in image segmentation: the statistical investigation of all detected contours. The structuring element of this opening procedure is a simple circle with a diameter of 19 pixels.

Following the initial processing, we applied iterative watershed-based dilation, which was once again under control of feedback object detection and compared to our model of a vessel for this species. We then generated several differently eroded shadow images before applying a watershed filter. The structuring element of the erosion was once again a circle. For our images, a diameter of 11 pixels worked best. For each element of the series, we increased the amount of iterations for which the erosion is

applied. In the first loop erosion was applied once, in the second twice and so forth. In each loop, the additional contours of sensible geometry were extracted after a watershed was applied to the region of interest. The markers of the watershed algorithm were defined by the pixel values received through both current erosion and dilation image. Five iterations were found to be sufficient for most of our samples (Fig. 3). The last step of our image segmentation for earlywood vessels was used to eliminate all objects which did not fit our model of “earlywood vessel”. The criteria are roundness, size and geometry (“circle”) and the confidence level was 90% similarity to each of our model parameters, namely geometry and area.



Fig. 3 Further structural image improvement was achieved after iterative opening and dilation was applied to the binary image. The vessels now appear clearer and minor disturbances are eliminated from the image. This process terminates the standard image

processing with white vessels on a black background. The *white* objects are now targets for our new analysis of automated tree-ring identification

Identification of earlywood vessels

One result of the image segmentation was an array of objects identified as most likely being earlywood vessels, as they fit to our model for an ideal vessel through pattern recognition at least at 90% identity. These are stored as an array of objects (earlywood vessels within the growth ring) including their shape and location.

Clusters through near neighbor analysis

The next step was to ascribe all identified vessel lumen to a specific tree ring. We sorted all vessels detected in ascending y-order. As we assumed that the wood probe was scanned with tree rings perpendicular to image height, and the medium diameter of a typical vessel for this probe was already established through the vessel detection in the previous step, we began our tree-ring reconstruction with the bottom-most vessel object furthest to the left of the image (Fig. 4). This initial element defines the very first tree-ring object by definition. Each vessel object scans its environment upwards in a sector which is n times its typical vessel geometry. This confidence range may be input to our analysis software. It was shown that this interval should not exceed the width of the latewood section of the probe. Each neighbor vessel detected within its confidence range was added as member of this tree-ring object. If no neighbor was found, that tree-ring object was closed and the next vessel which was not part of a tree-ring object began its scan of its environment as the first element of a new tree-ring object. At the end of this process, a certain number of tree rings and tree-ring fragments were detected (Fig. 4).

For some wood probes, large gaps between earlywood vessels of the same tree ring appear. One explanation for this could be vascular rays in oaks. After conducting the cluster analysis, our software performed an analysis of the

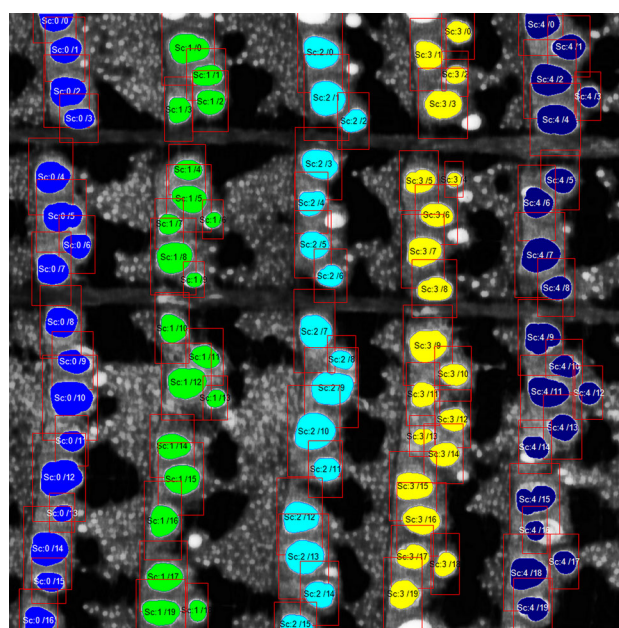


Fig. 4 Near neighbor analysis in a historical oak sample from construction timber (AD 1700). Area covered (*red rectangle*) to detect nearest neighbor vessels. Confidence sections in ranges of 1.3–2.5 times the mean diameter of earlywood vessels were applied. Detected fragments (superclusters) are denoted by the same color as individual tree rings. Each vessel is labeled (code within each vessel) for further analysis

clusters detected. “Unsafe” clusters were marked at this point. One criterion for identification of an unsafe cluster is, for example, the number of vessels within said cluster. The mean number of vessels within a cluster was established in the previous step. As a knowledge-based analysis system, we implemented a confidence interval of 0.90 at both ends of extreme values to be regarded as being safe. Unsafe clusters were omitted from further investigation, but were still included in the results (marked as “unsafe”).

Supercluster as tree-ring model

“Safe” clusters detected thus far were joined to superclusters in the second step of tree-ring reconstruction: an open-ended recursively working process. This process terminated when no more additional clusters could be added to a supercluster. Because joining clusters to each other is more difficult and versatile than joining vessels into a cluster, a more sophisticated algorithm is required. The decision whether a cluster may join a supercluster or not depends on several crucial criteria: (1) the cluster must be located above the supercluster (scanning always starts from bottom to top); (2) none of the cluster vessels may be located below any of the supercluster vessels (indicates a cluster to the left of the supercluster, which is not a member of the tree ring). In case of a ring-porous probe such as *Quercus* (or trees of similar wood anatomy), vascular rays may cross and interrupt a tree ring and may shift the tree-ring fragment above to the left or right. Therefore, the search for a most likely fragment of the supercluster must be more sophisticated than a simple regression extrapolation. In the current implementation of our software, we used a search pattern which utilized a specific strategy for detection (Fig. 5).

The search pattern reflected the varying likelihood of detecting a cluster above an existing supercluster at different risk levels. The size of the fields was defined by the average size of the top five vessels of the supercluster. It is strongly recommended not to use the mean size or mean geometry of an overall vessel as there is additional useful information within the top five vessels of the existing supercluster. As the vessels above a vascular ray (gap) belong to the ones within the already detected supercluster, shape analysis is a further search factor. In the first step, the top five vessels of the existing

superclusters were investigated. Their mean shape and size was calculated; the topmost vessel was determined and the extension of the supercluster at the top five levels measured. The base point to which the detection pattern snaps was calculated as the top y-coordinate of the supercluster and the geometric midpoint of the extension at the top of the supercluster. The fields (Fig. 5) then indicated to the area of the subcluster(s) to be investigated above. Field sizes are the mean of the top five level vessels within the supercluster multiplied by an extension value (which may be manually adjusted, but in most cases was 1.2 times the mid-geometry of the five top vessels of the supercluster). The cluster geometry was then compared to the supercluster geometry. If any vessel fell below (in the y-direction) any of the vessels within the supercluster, the whole cluster was not added to this supercluster as the cluster being located below and to the left of the supercluster is a forbidden structure for a tree ring. As the joining of superclusters was recursive, superclusters become subclusters with the next iteration, so that finally all clouds were superclusters (with the exception of the mistrusted ones). Figure 6 shows superclusters within a 5200-year-old subfossil oak tree.

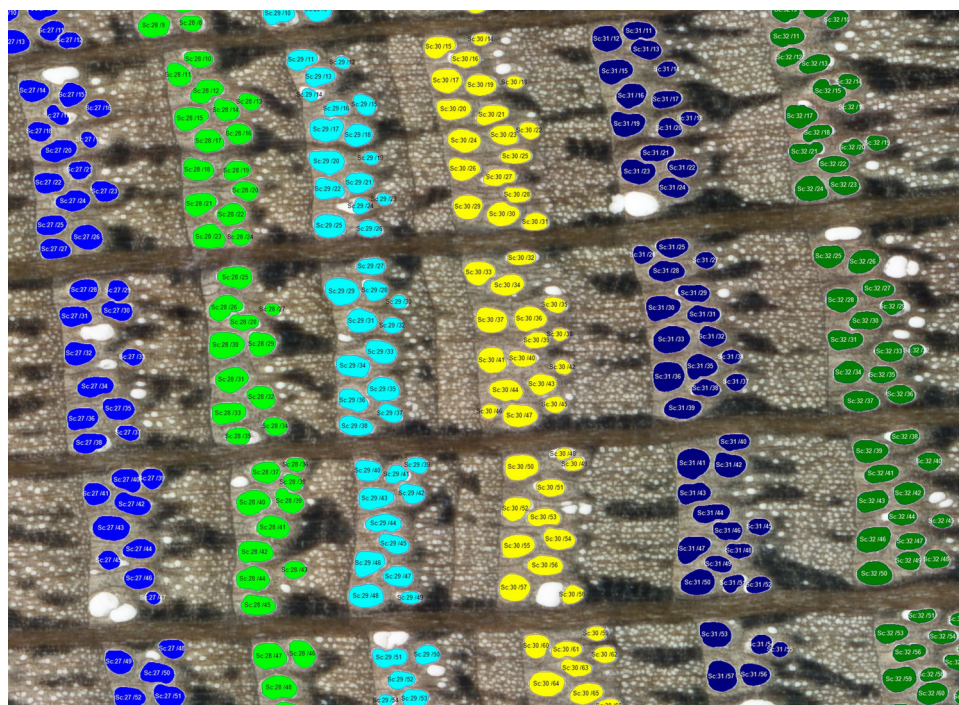
Generating results

The final step in image analysis was to generate tree-ring-based results and store these in a result file. As our software runs in batch mode, it is possible to automatically store all results as individual files (with the same name as the image) or in a single result file. Probe label (image name), number of detected tree rings and associated standard earlywood vessel parameters suited for climate reconstruction (e.g., arithmetic mean of cross-sectional area, standard deviation) are listed. The file format is compatible

Fig. 5 Search pattern for detection of clusters during supercluster analysis. Search starts from *bottom* (red element) and renders the elements in ascending order. That order is one strategy being used to keep false-positive detection as low as possible. In case one of these points detects a vessel within another cluster, the vessels within that cluster are further more investigated. If all of these clusters do not harm any rules, that cluster is regarded as being part of the currently investigated supercluster



Fig. 6 Segmented earlywood vessels within individual tree rings detected automatically in subfossil oak (3200 BC). Different colors denote superclusters of particular tree rings. Artifacts or vessels with incorrect contours (white elements) are recognized and excluded from further analysis



to Excel, so that further numerical evaluation could be conducted there.

Image-based high-volume analysis using samples from living oak trees

To stress test the CATS software living oak (*Quercus robur* L.), samples from the Hohenheim tree-ring archive were used. The trees originated from riparian forests which are economically managed within the Mainfranken region (southern Germany) and are located in the vicinity of the Main River. The trees are well water-supplied and flooding occurs regularly in winter, but rarely during the summer. The samples were taken from 22 adult individuals with an increment borer (2 cores per tree at breast height). The cores were fixed on wooden holders and the cross-sectional surface was smoothed with a core-microtome. Tyloses were removed from earlywood vessels using compressed air. To enhance the optical contrast, chalk was filled into the vessels before the cross section of each sample was scanned with a resolution of 4800 dpi (Epson Expression 10000 XL, Seiko Epson Corporation, Japan).

The samples used in this study to stress test CATS are part of the Holocene oak chronology (HOC) Hohenheim (located at University of Hohenheim) containing a large number of precisely dated ancient to modern trees spanning the entire Holocene (Friedrich et al. 2004). This collection has been used to address different questions regarding climate dynamics and environmental changes over the past

12 millennia (Friedrich et al. 2001, 2006; Land et al. 2015; Land 2014; Schönbein et al. 2015; Spurr et al. 2002).

Vessel chronologies and daily meteorological records for climate response analysis

The mean earlywood vessel area and median earlywood vessel area close to the tree-ring border were tested for their potential response to daily meteorological conditions. Similar to total-ring width series, vessel dimensions also show an age-related growth trend. This trend was removed by applying a cubic smoothing spline with 50% frequency–response cutoff at 10, 30 and 70% for each series (Cook and Peters 1981). Autocorrelation was removed and variance was stabilized before the corresponding chronologies were developed by using a biweight robust mean (hereafter referred to as Mean Spl10, Mean Spl30, Mean Spl70, Median Spl10, Median Spl30 and Median Spl70).

Expressed population signal (EPS) and mean inter-series correlation (RBAR) were calculated in a 50-year window with 25-year overlap. The standardization procedure was carried out with the software ARSTAN (Cook and Krusic 2006).

We used daily records from 1880 until present of the weather station Bamberg (49.88N, 10.92E) and the run-off gauge of Schweinfurt (50.04N, 10.24E), both located very near to the study site. Daily sum of precipitation and mean/minimum/maximum temperature (weather station Bamberg) were obtained from KNMI Climate Explorer (<https://>

climexp.knmi.nl) and the daily run-off data from the Bavarian Ministry for the Environment. Heat sum was calculated from the daily mean temperature data set. Daily mean temperature below +5 and +7.5 °C was not considered. All records were checked for missing data and the only gap was found in the temperature records (mean, minimum, maximum) for the year 1882 from May 9 to May 12. Thus the year 1882 was omitted from further analysis.

Climate response analysis

For the identification of sensitive periods, the vessel chronologies were compared to daily meteorological records. We developed a MATLAB® (The MathWorks® 2013) script that aggregates the meteorological data for each year altering (1) the length of the data interval used for correlation (from 11 to 111 days in steps of five days) and (2) the starting date of the data derived from (1) between January 1 and December 15 (Schönbein 2011). A Pearson correlation between each newly generated meteorological series and each vessel chronology was calculated. This step was done for the entire time period from 1880 to 2004 (number of trees ≥ 11). Statistical significance was attained when the level of significance was below $p < 0.01$. To evaluate changes in temporal sensitivity and consistency, a response analysis was performed for eleven 20-year (e.g., 1905–1924, 1935–1954) and three 62-year-long overlapping sub-periods (e.g., 1913–1974) to evaluate changes in temporal sensitivity and consistency.

Results

Vessel measurements and chronologies

The raw and indexed measurements of the mean (Fig. 7a, b) and median (Fig. 7e, f) vessel sizes, the developed vessel chronologies (Fig. 7c, g), the number of earlywood cells per year included for the mean vessel size measurements (Fig. 7d) as well as the number of trees (Fig. 7h) are displayed in the corresponding figures. The calculated mean EPS for all six maintained chronologies is high (1885–1985). The lowest mean EPS and mean RBAR was obtained for Mean Spl10 (EPS = 0.78, RBAR = 0.16) and the highest for Median Spl70 (EPS = 0.87, RBAR = 0.27). The lowest 50-year window EPS is found for Mean Spl10 from 1885 to 1935 and from 1935 to 1985 (EPS = 0.76), the highest for Median Spl70 from 1910 to 1960 (EPS = 0.90). In the years 1912, 1940 and 1948 the vessel sizes decreased rapidly in many trees.

The corresponding chronologies of mean versus median vessel area are highly correlated for the period between

1880 and 2004 (Spl10: $r = 0.79$, Spl30: $r = 0.86$, Spl70: $r = 0.85$). All chronologies show a low variability from 1950 onwards.

Climate–response analysis

Based on the daily meteorological data, the performed climate–response analysis revealed a large quantity of results. Here the highest relationships for the entire period (1880–2004) and for several sub-periods (e.g., 1913–1974, 1885–1904) are shown.

The highest correlation during the entire observation period of 1880–2004 between vessel chronology and climate parameter is found for Mean Spl30 and the heat sum (>7.5 °C) between March 14 and April 18 ($r = 0.34$, $p < 0.01$, $N = 124$) (Fig. 8a). The second highest correlation is obtained for Median Spl10 and the heat sum (>7.5 °C) between March 17 and April 16 ($r = 0.32$, $p < 0.01$, $N = 124$) (Fig. 8b). Periods of high consistency (e.g., 1916–1923) as well as low (e.g., 1906–1914) are obvious. The pronounced long-term trend in the heat sum series (very distinct from 1880 until 1920) could reduce the response. The MATLAB® script used makes no allowance for that as the raw data record is used to conduct the analysis. Thus in a second step, the raw record of the heat sum was detrended (low-pass filter) to remove the long-term portion. Both the detrended series of the heat sum and the mean Spl30 were z-transformed and the correlation coefficient was calculated. The correlation coefficient increased only slightly to $r = 0.36$ ($p < 0.01$) (Fig. 9a, b). Analyzing the mid-frequency (band-pass filter = 0.17–0.03 Hz) of both records (Fig. 9c), a high consistency can be observed ($r = 0.47$, $p < 0.01$), which is higher in the first part of the analysis (until the 1940s) but lower in the second period. While the two time series remain highly consistent from 1880 to 1905, a shift of 2 years can be identified between the 1910s and 1940s. From 1945 to 2004 only a weak coherence exists.

Results for minimum and maximum temperature show highly positive relationships, whereas precipitation and run-off data revealed less significant negative correlations.

Temporal changes of vessel response

To investigate the temporal consistency between the two vessel chronologies (Mean Spl30, Median Spl10) and the heat sum during the entire period, an analysis was carried out for three 62-year-long as well as for 20-year-long overlapping sub-periods. Table 1 displays the results for the analysis of the vessel chronologies Mean Spl30 and Median Spl10 and the heat sum (>7.5 °C) within the three overlapping 62-year sub-periods 1880–1942, 1913–1974 and 1943–2004. The vessels respond positively to the heat sum in spring for all three

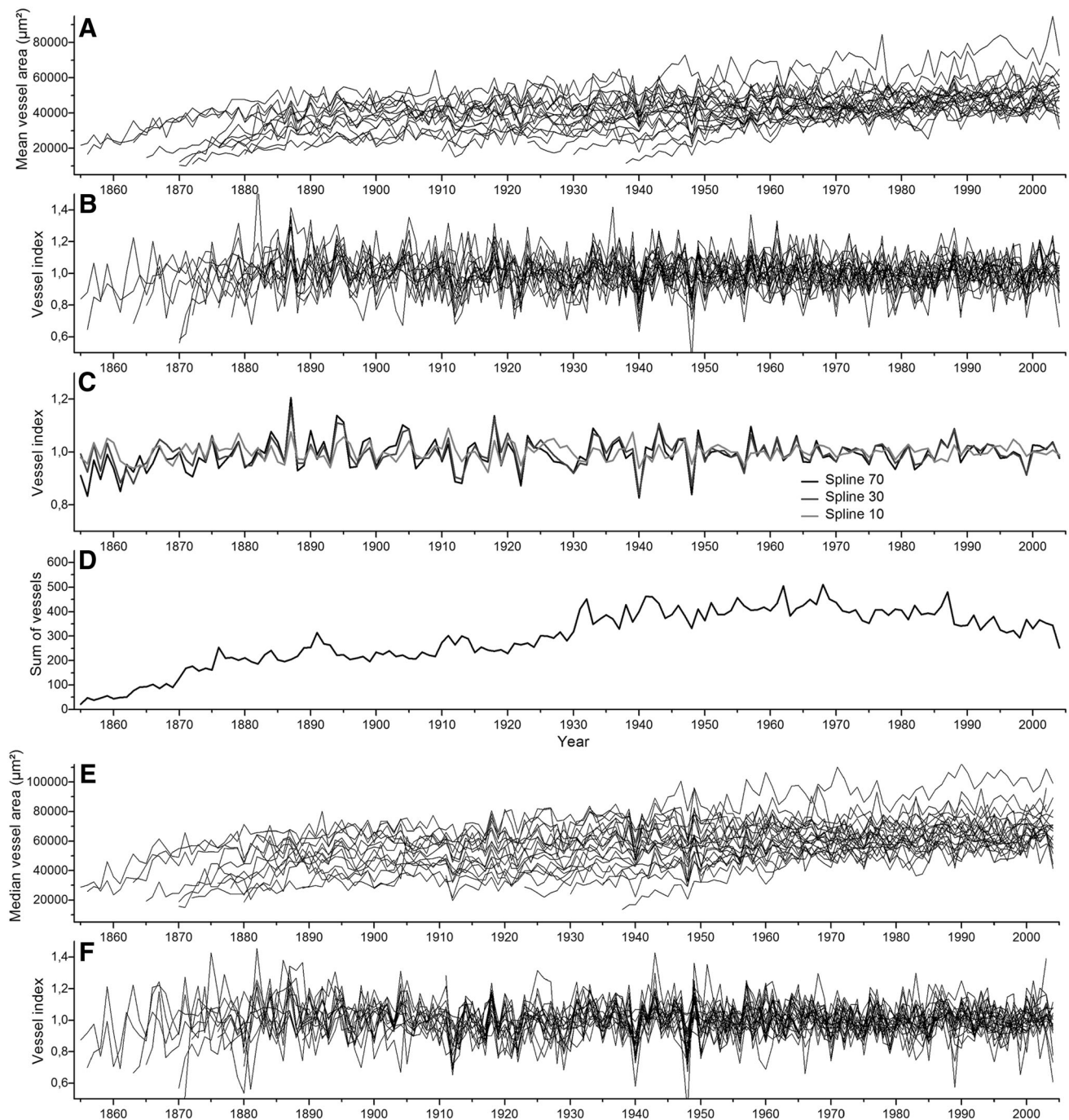


Fig. 7 **a** Annual mean cross-sectional earlywood vessel area (μm^2) for 22 trees. **b** Indexed (Spline 70) series of **a**. **c** Index chronologies of mean vessel area using different standardization procedures (Spline 10, Spline 30, Spline 70). **d** Number of vessels per year included in the measurement. **e** Annual median cross-sectional earlywood vessel

area (μm^2) from 22 trees. **f** Indexed (Spline 70) series of **e**. **g** Index chronologies of median vessel area using different standardization procedures (Spline 10, Spline 30, Spline 70). **h** Number of trees per year (replication) and the period of climate response analysis (gray bar) from 1880 to 2004

62-year sub-periods. In the sub-periods 1880–1942 and 1913–1974 the earlywood vessels are significantly ($p < 0.01$) influenced by the heat sum between March 17 and April 16. The relationship is much stronger during the sub-period 1913–1974 ($r = 0.48$, $r = 0.50$) than during 1880–1942

($r = 0.37$, $r = 0.35$). From 1943 to 2004, the correlation coefficient decreases to $r = 0.36$ ($p < 0.01$) and $r = 0.32$ ($p < 0.05$), while the length of the sensitive interval for Mean Spl30 doubles: February 27 to May 3. The sensitive interval for Median Spl10 remains consistent (March 14–April 18).

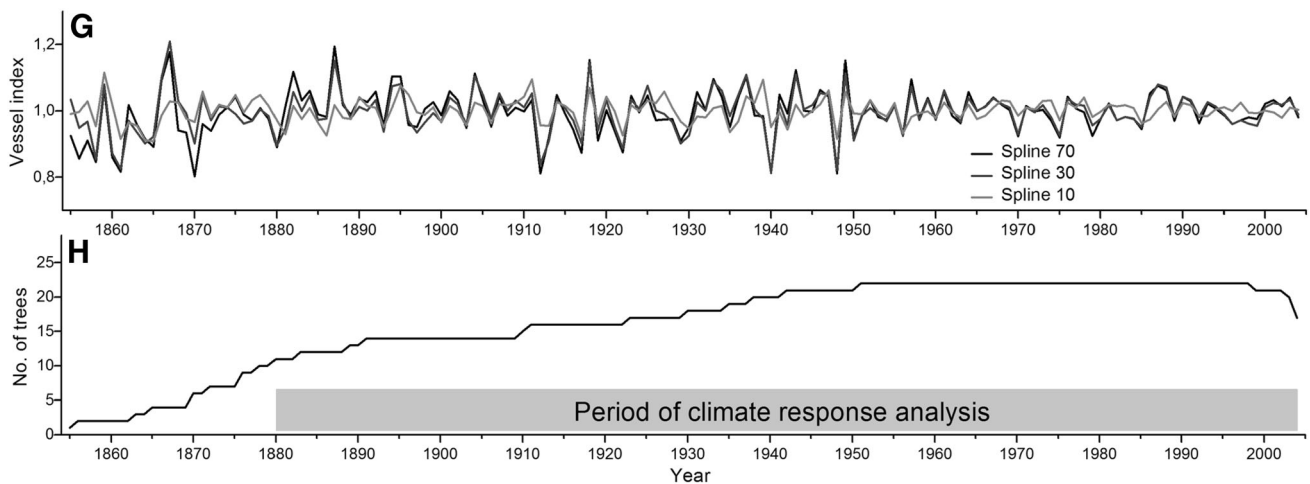


Fig. 7 continued

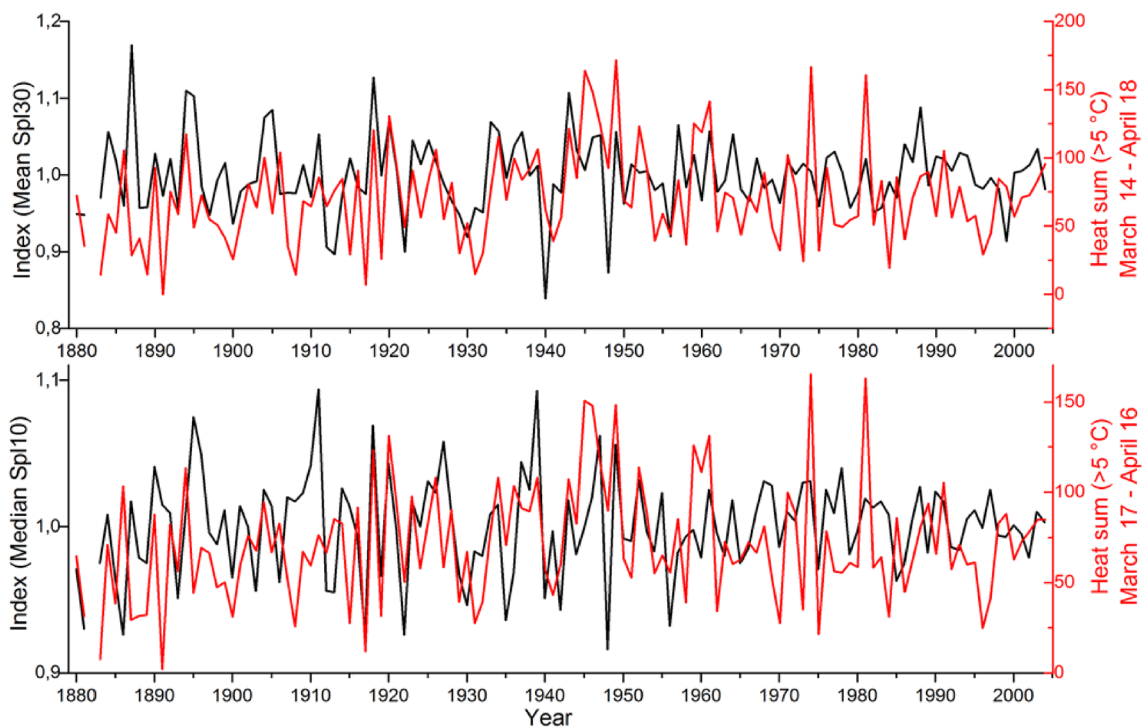


Fig. 8 Line graphs of the response analysis. **a** Best relationship between mean vessel area chronology (Mean Spl30, black) and heat sum from March 14 to April 18 (calculated from daily mean temperature data >7.5 °C, red) from 1880 to 2004 ($r = 0.34$, $p < 0.01$). **b** Best relationship between median vessel area chronology

(Median Spl10, black) and heat sum from March 17 to April 16 (red) ($r = 0.32$, $p < 0.01$). Due to several missing records in the daily temperature data of the year 1882 (from May 9 to May 12), this year was omitted in the response analysis

The consistency of the vessel–heat sum relationships found for the chronologies Mean Spl30 (March 14–April 18) and Median Spl10 (March 17–April 16) had been analyzed for eleven 20-year overlapping sub-periods. In four sub-periods between 1915 and 1964, the two vessel chronologies reveal high significance to the corresponding heat sum record (Fig. 10) at a significance level of $p > 0.05$. During

the sub-periods 1885–1924 and 1955–2004, no significant response between the two vessel chronologies and the corresponding intervals could be determined.

From 1925 to 1954, a significant negative relationship ($r = -0.76$, $p < 0.01$, $N = 30$) between the chronology Mean Spl30 and the heat sum in winter (November 7–February 15) was found.

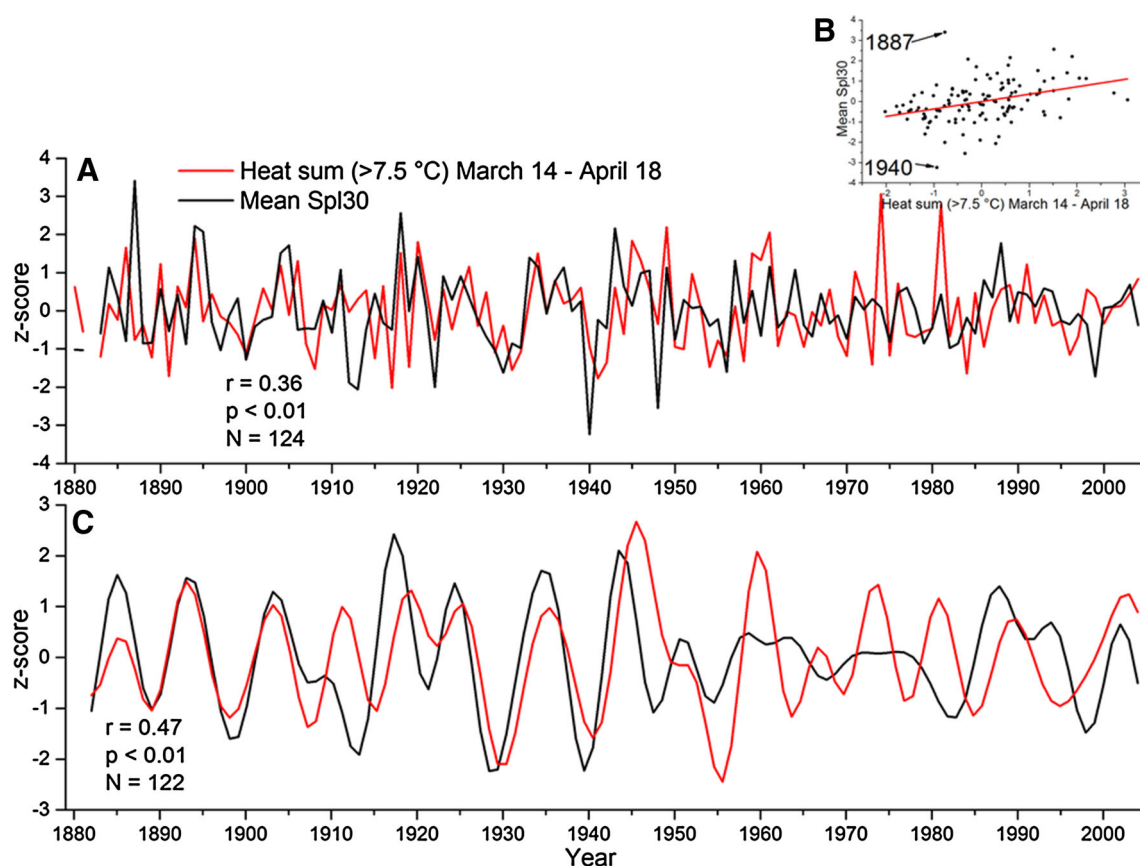


Fig. 9 **a** Mean vessel area chronology (Mean Spl30, black) and heat sum from March 14 to April 18 (red) after the long-term trend was eliminated. Both time series are z -transformed. The statistical relationship increases slightly to $r = 0.36$ ($p < 0.01$, $N = 124$) compared to the response calculation from Fig. 8. **b** Comparison of

mid-frequency pattern (band-pass filter = 0.17–0.03 Hz) of the two time series ($r = 0.47$, $p < 0.01$, $N = 122$). From 1883 to 1950 the correlation between the vessel chronologies and the heat sum from mid-March to mid-April is much more pronounced than for the time period from 1950 to 2004

Table 1 Sensitivity of the two vessel chronologies (Mean Spl30 and Median Spl10) to seasonal heat sum in the 62-year sub-periods ($p < 0.05$)

Period	Mean Spl30 interval (r)	Median Spl10 interval (r)
1880–1942	March 17–April 16 (0.37)	March 17–April 16 (0.35)
1913–1974	March 17–April 16 (0.48)	March 17–April 16 (0.50)
1943–2004	February 27–May 5 (0.36)	March 14–April 18 (0.32)

Correlation coefficients are indicated in brackets. During the sub-period 1913–1974 both chronologies respond much better ($r = 0.48$, $r = 0.50$) to heat sum than during 1880–1942 ($r = 0.37$, $r = 0.35$) and 1943–2004 ($r = 0.36$, $r = 0.32$)

Discussion

We present the application of a new computer-aided tree-ring analysis software (CATS) for high-volume analysis of vessel sizes. In this study, the freeware automated tool was applied to analyze two common earlywood vessel parameters in 22 oak trees (*Q. robur* L.) using long-term climate data sets. The vessel chronologies were correlated with

daily meteorological records from nearby climate and run-off station. The vessel size chronologies demonstrated a very similar behavior in the climate–growth analysis. The earlywood vessel chronologies (Mean Spl30 and Median Spl10) yielded a positive response to the heat sum (>7.5 °C) in spring (March 14–April 18 and March 17–April 16) during the entire investigated period from 1880 to 2004. Vessel parameters also showed a slightly less significant response to maximum daily temperature in spring. Several studies about earlywood vessel lumen area on *Q. robur* report positive temperature signals in spring (e.g., Matison and Dauškanė 2009), in winter (e.g., Pritzkow et al. 2016), in winter–spring (Tumajer and Trembl 2016) as well as a negative precipitation signal during the autumn–winter period (González-González et al. 2015). Studies of other *Quercus* species often reveal a clear response to precipitation (e.g., Fonti et al. 2009; González-González et al. 2014). Our findings agree with the studies showing a direct positive correlation of temperature and earlywood vessel size during the time of formation in spring. Several physiological explanations of vessel–temperature

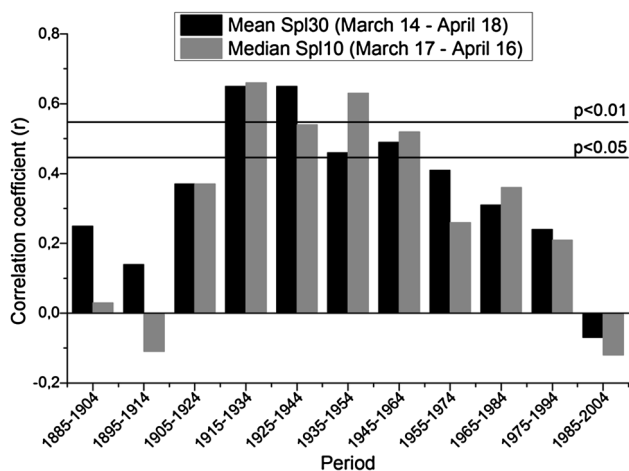


Fig. 10 Response analysis for eleven 20-year overlapping sub-periods between the mean vessel area chronology (black) and the heat sum from March 14 to April 18 (calculated from daily mean temperature data >7.5 °C) as well as between the median vessel area chronology (gray) and the heat sum from March 17 to April 16. Significance level of $p < 0.01$ and $p < 0.05$ are labeled. During the sub-periods 1915–1934, 1925–1944, 1935–1954 and 1945–1964 the two vessel chronologies show highly significant correlations with the heat sum

interactions have been discussed in other publications (e.g., Aloni 2015; González-González et al. 2014; Pritzkow et al. 2016). An influence of stem temperature reaching a threshold of 5 °C with a delay of 1–2 weeks before cambial activity begins has been reported by Güney et al. (2016) in Lebanon cedar and Kudo et al. (2014) found that cambial reactivation in the ring-porous hardwood *Quercus serrata* is triggered mainly by temperature. The detected close relationship of air heat sum seems to initialize cambial activity and earlywood vessel development directly in a positive manner. Rising heat sum in spring may lead to larger vessels by changing the plant hormonal status for cambial tissue (Aloni 2015).

The climate–response analysis for sub-periods (e.g., 20-year), showed that the relationship between vessel sizes and mid-March to mid-April heat sum is strongly evident during the years from 1915 until 1964. From 1925 to 1954, a strong negative relationship between the heat sum during winter (November 7–February 15) and mean vessel area is evident. During these years, winter conditions in Central Europe had been very harsh (e.g., below -20 °C in 1925, 1929, 1939, 1940, 1942). This supports the hypothesis that severely cold winter temperatures stress cambial cell initials (Aloni 2015) and could lead to smaller vessels in the following growing season. The noticeably reduced variability of vessel sizes during the past five decades (from 1955 onwards) cannot be explained by forest management activities or changes in the run-off regime. The documented massive insect attacks of the green oak leaf roller

(*Tortrix viridana* L.) in this region (in the years 1948 and 1954–1958) also provide, to our best knowledge, no explanation for this reduction and thus the reason remains unclear. Pritzkow et al. (2016) detected a very strong positive winter temperature response from 1951 to 2010 for pedunculate oak trees from northern Poland. For the same period, the vessel sizes of our study show a weak but significant ($p < 0.05$) response.

Our results show that a temporal aspect is crucial when investigating climate–vessel relationships, meaning that more quantity of climate–vessel studies should be performed in the near future in general. To this end, our novel computer-aided tree-ring image analysis software CATS (freeware) will aid in performing such analysis in a reasonable time frame.

Future enhancements of CATS and outlook

Technical evolution clearly shows that images of significantly higher resolution can be captured from innovative microscopic techniques in the future, such as two-photon laser scanning microscopy which offers large-scale screening of images. Thus, CATS can also be applied for latewood-cell analysis which is currently not feasible due to insufficient image quality and resolution, thereby enabling analysis of these features in large-scale projects. The necessary basis for quantitative latewood-cell analysis is already included in CATS, which would allow efficient analysis of whole tree rings. Time-consuming manual detection of tree-ring boundaries, identification and elimination of preparation-induced artifacts by the user will be fully automated.

From a dendroclimatological point of view, CATS will be improved in terms of species-specific analysis by adding species-specific wood-anatomical characters from a database at the beginning of the measurement process to make analysis much more efficient. One further software project (ELiA ∞) will soon be completed and will be available for common and royalty-free download at <http://www.elia8.org> when launched. This ExpertSystem for Light Microscopy integrates a highly complex relational database system for both data annotation and biosystematics. ELiA ∞ includes ELiA (which is an offline but updateable biosystematics database and interface for annotation of more than 680,000 taxa), which incorporates automated internet-based data mining support. As ELiA and ELiA ∞ are connected by crosstalk, we will work hard to implement an automated database search of currently investigated wood probes: CATS will annotate its results through the relational database system of ELiA ∞ . We plan to use ELiA ∞ 's data crosstalk to ELiA for automated, internet-based data mining to verify and improve climate data

reconstruction. This approach and its progress will be described in further publications.

The next evolution-step will push CATS into complete tree-ring analysis using millennial-aged subfossil and historical oak samples. CATS is, along with some sample images, available for common download at <http://www.hs-emden-leer.de/softlinks/catrassupplementalkauerlandzip.html>.

Conclusions

Computer-aided tree-ring analysis software is our first automated software which analyzes wood probes using image analysis to obtain high volumes of dendroclimatically relevant data. The image analysis workflow has proved to be suitable for automated tree-ring detection. A stress test using images of distinct tree rings from 22 living oak samples has shown that this software approach is suitable for quantitative cell-size measurements. In the case of very narrow tree rings, the fully automated reconstruction may generate some mismatched superclusters which should be corrected manually. Further improvements for such issues are a focal point in current software development.

The climate growth analysis over the entire period (1880–2004) using two vessel chronologies in combination with a long-term daily meteorological record reveal that the occurrence of larger cross-sectional surface areas of the vessels are positively correlated with the heat sum between mid-March to mid-April. This effect is particularly pronounced for five decades in the twentieth century (1915–1964).

Using daily meteorological records to conduct climate–vessel analysis is highly recommended as trees respond with cambial activity to climatic and hydrologic effects and are decoupled from monthly records and thus a more precise analysis can be obtained.

Availability and requirements

- Project name: CATS.
- Operating system: Windows 7, Windows 10, 64Bit.
- Programming language: C#, .NET.
- Other requirements: computer should be able to run OpenGL/OpenCv.
- License: experimental academic software. Royalty-free, non-exclusive.
- Download: <http://www.hs-emden-leer.de/softlinks/catrassupplementalkauerlandzip.html>.

Author contribution statement AL and GK wrote the manuscript and all authors reviewed and revised the manuscript. GK, MW, KUR

and SE developed the main part of CATS. AL and DR performed the high-volume cell-size measurements and conducted the response analysis. The authors read and approved the final manuscript.

Acknowledgements We are grateful to Margaret Janke and Reiner Zimmermann for their assistance in reviewing this article. The authors thank the anonymous reviewers for valuable comments on an earlier draft of the manuscript.

Compliance with ethical standards

Funding This work was supported by the University of Hohenheim and University of Applied Sciences Emden-Leer by travelling support.

Conflict of interest The authors declare that they have no conflict of interest.

Open Access This article is distributed under the terms of the Creative Commons Attribution 4.0 International License (<http://creativecommons.org/licenses/by/4.0/>), which permits unrestricted use, distribution, and reproduction in any medium, provided you give appropriate credit to the original author(s) and the source, provide a link to the Creative Commons license, and indicate if changes were made.

References

- Aloni R (2015) Ecophysiological implications of vascular differentiation and plant evolution. *Trees* 29:1–16
- Büntgen U, Tegel W, Nicolussi K, McCormick M, Frank D, Trouet V, Kaplan JO, Herzig F, Heussner KU, Wanner H, Luterbacher J, Esper J (2011) 2500 years of European climate variability and human susceptibility. *Science* 331:578–582
- Cook ER, Krusic PJ (2006) ARSTAN4.1_XP. <http://www.Ideo.columbia.edu>
- Cook ER, Peters K (1981) The smoothing spline: a new approach to standardizing forest interior tree-ring width series for dendroclimatic studies. *Tree Ring Bull* 41:45–53
- Cousty J, Bertrand G, Couprie M, Najman L (2006) Fusion graphs, region merging and watersheds. In: Kuba A, Nyúl LG, Palágyi K (eds) *Discrete geometry for computer imagery*. Springer, Berlin, pp 343–354
- Esper J, Schneider L, Krusic PJ, Luterbacher J, Büntgen U, Timonen M, Sirocko F, Zorita E (2013) European summer temperature response to annually dated volcanic eruptions over the past nine centuries. *Bull Volcanol* 75:1–14
- Fonti P, García-González I (2008) Earlywood vessel size of oak as a potential proxy for spring precipitation in mesic sites. *J Biogeogr* 35:2249–2257
- Fonti P, Eilmann B, García-González I, von Arx G (2009) Expeditious building of ring-porous earlywood vessel chronologies without losing signal information. *Trees* 23:665–671
- Fonti P, von Arx G, García-González I, Eilmann B, Sass-Klaassen U, Gärtner H, Eckstein D (2010) Studying global change through investigation of the plastic responses of xylem anatomy in tree rings. *New Phytol* 185:42–53
- Friedrich M, Kromer B, Kaiser KF, Spurk M, Hugen KA, Johnsen SJ (2001) High-resolution climate signals in the Bølling–Allerød Interstadial (Greenland Interstadial 1) as reflected in European tree ring chronologies compared to marine varves and ice-core records. *Quat Sci Rev* 20:1223–1232
- Friedrich M, Remmele S, Kromer B, Spurk M, Hofmann J, Hurni JP, Kaiser KF, Küppers M (2004) The 12,460-year Hohenheim oak

- and pine tree ring chronology from Central Europe—a unique annual record for radiocarbon calibration and palaeoenvironment reconstructions. *Radiocarbon* 46:1111–1122
- Friedrich WL, Kromer B, Friedrich M, Heinemeier J, Pfeiffer T, Talamo S (2006) Santorini eruption radiocarbon dated to 1627–1600 B.C. *Science* 312:548
- González-González BD, Rozas V, García-González I (2014) Early-wood vessels of the sub-Mediterranean oak *Quercus pyrenaica* have greater plasticity and sensitivity than those of the temperate *Q. petraea* at the Atlantic-Mediterranean boundary. *Trees* 28(1):237–252. doi:[10.1007/s00468-013-0945-2](https://doi.org/10.1007/s00468-013-0945-2)
- González-González BD, Vázquez-Ruiz RA, García-González I (2015) Effects of climate on earlywood vessel formation of *Quercus robur* and *Q. pyrenaica* at a site in the northwestern Iberian Peninsula. *Can J Forest Res* 45:698–709. doi:[10.1139/cjfr-2014-0436](https://doi.org/10.1139/cjfr-2014-0436)
- Güney A, Küppers M, Rathgeber C, Sahin M, Zimmermann R (2016) Intra-annual stem growth dynamics of Lebanon Cedar along climatic gradients. *Trees*. doi:[10.1007/s00468-016-1492-4](https://doi.org/10.1007/s00468-016-1492-4)
- Kniesel BM, Günther B, Roloff A, von Arx G (2015) Defining ecologically relevant vessel parameters in *Quercus robur* L. for use in dendroecology: a pointer year and recovery time case study in Central Germany. *Trees* 29:1041–1051
- Kudo K, Nabeshima E, Begum S, Yamagishi Y, Nakaba S, Oribe Y, Yasue K, Funada R (2014) The effect of localized heating and disbudding on cambial reactivation and formation of earlywood vessels in seedlings of the deciduous ring-porous hardwood, *Quercus serrata*. *Ann Bot* 113:1021–1027
- Land A (2014) Holzanatomische Veränderungen als Reaktion auf extreme Umwelt Ereignisse in rezenten und subfossilen Eichen und deren Verifizierung im Experiment, Dissertation. University of Hohenheim, Hohenheim
- Land A, Schönbein J, Friedrich M (2015) Extreme climate events identified by wood-anatomical features for the Main region (Southern Germany)—a case study for 3000–2000 BC. In: Meller H, Arz HW, Jung R, Risch R (eds) 2200 BC—a climatic breakdown as a cause for the collapse of the old world? Landesamt für Denkmalpflege und Archäologie Sachsen-Anhalt, Landesmuseum für Vorgeschichte, Halle (Saale), pp 595–602
- Leuschner HH, Sass-Klaassen U, Jansma E, Baillie MGL, Spurk M (2002) Subfossil European bog oaks: population dynamics and long-term growth depressions as indicators of changes in the Holocene hydro-regime and climate. *Holocene* 12:695–706
- Matison R, Dauškanė I (2009) Influence of climate on earlywood vessel formation of *Quercus robur* at its northern distribution range in central regions of Latvia. *Acta Univ Latv* 753:49–58
- Otsu N (1979) A threshold selection method from gray-level histograms. *IEEE Trans Syst Man Cybern* 9:62–66
- Peng H (2008) Bioimage informatics: a new area of engineering biology. *Bioinformatics* 24:1827–1836
- Pritzkow C, Wazny T, Heußner KU, Słowiński M, Bieber A, Dorado Liñán I, Helle G, Heinrich I (2016) Minimum winter temperature reconstruction from average earlywood vessel area of European oak (*Quercus robur*) in N-Poland. *Palaeogeogr Palaeoclimatol Palaeoecol* 449:520–530
- Schönbein J (2011) Zur Rekonstruktion von Hochwasserereignissen in Europa aus holzanatomischen Parametern und historischen Quellen, Dissertation. University of Freiburg, Freiburg
- Schönbein J, Land A, Friedrich M, Glaser R, Küppers M (2015) Seasonal reconstruction of summer precipitation variability and dating of flood events for the millennium between 3250 and 2250 years BC for the Main region, Southern Germany. In: Schulz M, Paul A (eds) Integrated analysis of interglacial climate dynamics (INTERDYNAMIC), Springer Briefs in Earth System Sciences. Springer International Publishing, New York, pp 127–131
- Seftigen K, Linderholm HW, Drobyshev I, Niklasson M (2013) Reconstructed drought variability in southeastern Sweden since the 1650s. *Int J Climatol* 33:2449–2458
- Spurk M, Friedrich M, Hofmann J, Remmele S, Frenzel B, Leuschner HH, Kromer B (1998) Revisions and extensions of the Hohenheimer oak and pine chronologies—new evidence about the timing of the Younger Dryas/Preboreal-Transition. *Radiocarbon* 40:1107–1116
- Spurk M, Leuschner HH, Baillie MGL, Briffa KR, Friedrich M (2002) Depositional frequency of German subfossil oaks: climatically and non-climatically induced fluctuations in the Holocene. *Holocene* 12:707–715
- St. George S (2014) An overview of tree ring width records across the Northern Hemisphere. *Quat Sci Rev* 95:132–150
- The MathWorks® (2013) MATLAB, Natick
- Tumajer J, Treml V (2016) Response of floodplain pedunculate oak (*Quercus robur* L.) tree-ring width and vessel anatomy to climatic trends and extreme hydroclimatic events. *Forest Ecol Manag* 379:185–194
- Wilson R, Miles D, Loader NJ, Melvin T, Cunningham L, Cooper R, Briffa KR (2013) A millennial long March–July precipitation reconstruction for southern-central England. *Clim Dyn* 40:997–1017